A heuristic attempt to reduce transverse shear locking in fully integrated hexahedra with poor aspect ratio

Dr. Thomas Borrvall

Engineering Research Nordic AB

Linköping, Sweden

Summary:

In an attempt to alleviate transverse shear locking in fully integrated hexahedra elements with poor aspect ratio, two new variants of solid element type 2 in LS-DYNA have been developed, implemented and tested on some critical problems. The approach is based on modifying the jacobian matrix in such a way that the spurious stiffness is reduced without affecting the true physical behavior of the element. The method is in a sense justified by means of a theoretical motivation, but above all indicated to be of practical use through some illustrating examples. The two new solid elements are denoted type (ELFORM) -1 and -2 on the *SECTION_SOLID card, where the latter is more rigorous but suffers from a higher computational expense, whereas solid element type -1 has an efficiency slightly worse than solid element type 2 for explicit analyses. However, all three element types are in that sense comparable for large scale implicit analyses.

Keywords:

Selective reduced integration, hexahedron, transverse shear locking

1 Introduction

The constant stress brick element in combination with a suitable hourglass formulation, see [1] and references therein, is usually the preferred choice for large scale numerical modelling of solid structures in industrial applications because of its efficiency and sufficient accuracy. With this strategy however there remains the delicate choice of hourglass formulation and optimal values of associated parameters in order to get reliable results. Furthermore, numerical simulation projects often involve several stages corresponding to different types of analyses. This may require manual intervention during the process such as switching element formulation in between stages due to difference in character of the different types of analyses. An impact analysis may for instance be preceeded by a static (gravitational) loading analysis and followed by an implicit springback analysis. Element formulations typically possess different stiffness properties, and this could make it difficult to validate the overall results in a consistent way. From an engineering point of view it is of interest to strive for a numerical modelling concept that is generically applicable and that minimizes these types of hands-on operations. A modelling strategy in this direction would be to consequently use a fully integrated brick element in favour of the constant stress element, even though this means sacrificing numerical efficiency, but this is generally not recommended since this element is regarded too stiff in most situations. In particular this is the case when the elements exhibit poor aspect ratio, i.e., when one element dimension is significantly smaller than the other(s). This occurs for instance when modelling thin walled structures and the time for solving the problem prevents using a sufficient number of elements for maintaining close to cubic elements throughout the structure. The reason for the locking phenomenon is that the element is not able to represent pure bending modes without introducing transverse shear strains, and this may be bad enough to lock the element to a great extent. In an attempt to solve this transverse shear locking problem, two new fully integrated solid elements are introduced and documented herein that hopefully may become of practical use for these types of applications. The rest of the paper is organized as follows. In Section 2 the theory for the fully integrated brick element is given in order to illustrate the transverse shear locking anomaly in Section 3. This is used as a base for formulating the theory of the new solid elements in Sections 4 and 6, for which the alleviation of the transverse shear stiffness is illustrated in Section 5. In Section 7 numerical examples are presented that show their practical usage and the paper ends with some concluding remarks in Section 8.

2 Brief theory of fully integrated solid element type 2

Let x_{Ii} represent the nodal coordinate of dimension i and node I, and likewise v_{Ii} its velocity. Furthermore denote

$$N_I(\xi_1, \xi_2, \xi_3) = \frac{1}{8}(1 + \xi_1^I \xi_1 + \xi_2^I \xi_2 + \xi_3^I \xi_3 + \xi_{12}^I \xi_1 \xi_2 + \xi_{13}^I \xi_1 \xi_3 + \xi_{23}^I \xi_2 \xi_3 + \xi_{123}^I \xi_1 \xi_2 \xi_3)$$

the shape functions for the standard isoparametric domain where

$$\xi_1^* = \begin{bmatrix} -1 & 1 & 1 & -1 & -1 & 1 & 1 & -1 \end{bmatrix}$$
$$\xi_2^* = \begin{bmatrix} -1 & -1 & 1 & 1 & -1 & -1 & 1 & 1 \end{bmatrix}$$
$$\xi_3^* = \begin{bmatrix} -1 & -1 & -1 & -1 & 1 & 1 & 1 & 1 \end{bmatrix}$$
$$\xi_{12}^* = \begin{bmatrix} 1 & -1 & 1 & -1 & 1 & -1 & 1 & -1 \end{bmatrix}$$
$$\xi_{23}^* = \begin{bmatrix} 1 & 1 & -1 & -1 & -1 & -1 & 1 & 1 \end{bmatrix}$$
$$\xi_{13}^* = \begin{bmatrix} 1 & -1 & -1 & 1 & -1 & 1 & 1 & -1 \end{bmatrix}$$
$$\xi_{123}^* = \begin{bmatrix} -1 & 1 & -1 & 1 & 1 & -1 & 1 & -1 \end{bmatrix}$$

and let furthermore

$$\xi_{21}^I = \xi_{12}^I$$
$$\xi_{32}^I = \xi_{23}^I$$
$$\xi_{31}^I = \xi_{13}^I.$$

The isoparametric representation of the coordinates of a material point in the element is then given as (where the dependence on ξ_1, ξ_2, ξ_3 is suppressed for brevity)

$$x_i = x_{Ii} N_I$$

and its associated jacobian matrix is

$$J_{ij} = \frac{\partial x_i}{\partial \xi_j} = x_{Ii} \frac{1}{8} \left(\xi_j^I + \xi_{jk}^I \xi_k + \xi_{jl}^I \xi_l + \xi_{123}^I \xi_k \xi_l \right),$$

where $k = 1 + \mod(j,3)$ and $l = 1 + \mod(j+1,3)$, i.e., no sum over k or l. For future reference let

$$J_{ij}^0 = x_{Ii}(0) \frac{1}{8} \xi_j^I$$

be the jacobian evaluated in the element center and in the beginning of the simulation (i.e., at time zero). The velocity gradient computed directly from the shape functions and velocity components is

$$L_{ij} = \frac{\partial v_i}{\partial x_j} = \dot{J}_{ik} J_{kj}^{-1} = B_{ijIk} v_{Ik}$$

where

$$B_{ijIk} = \frac{\partial N_I}{\partial \xi_l} J_{lj}^{-1} \delta_{ik}$$

is the gradient-displacement matrix and represents the element except for the alleviation of volumetric locking. To do just that, let

$$B_{ijIk}^0 = B_{ijIk}(0,0,0),$$

i.e., the gradient-displacement matrix evaluated at the element center, and construct the gradient-displacement matrix used for the element as

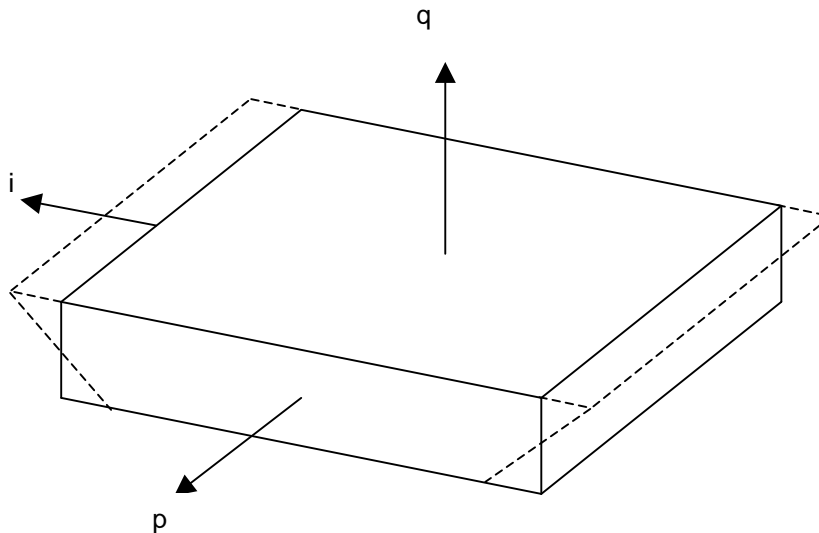$$\overline{B}_{ijIk} = B_{ijIk} + \frac{1}{3}(B_{llIk}^0 - B_{llIk})\delta_{ij}$$

Figure 1 Illustration of bending of a parallelepiped

3 Transverse shear locking example

To get the idea of the modifications needed to alleviate transverse shear locking, let's look at a parallelepiped of dimensions $l_1 \times l_2 \times l_3$. For this simple geometry the jacobian matrix is diagonal and the velocity gradient is expressed as (no sum over j)

$$\frac{\partial v_i}{\partial x_j} = \frac{2}{l_j} J_{ij} = \frac{1}{4l_j} v_{Ii} \left(\xi_j^I + \xi_{jk}^I \xi_k + \xi_{jl}^I \xi_l + \xi_{123}^I \xi_k \xi_l \right)$$

where, again, $k = 1 + \mathrm{mod}(j,3)$ and $l = 1 + \mathrm{mod}(j+1,3)$. Now let $i \neq p \neq q \neq i$, then a pure bending mode in the plane with normal in direction q and about axis p is represented by (see Figure 1 for an illustration of this mode)

$$v_{Ii} = \xi_{iq}^I$$
$$v_{Ip} = 0$$
$$v_{Iq} = 0$$

and thus the velocity gradient is given as

$$\frac{\partial v_i}{\partial x_j} = \frac{1}{4l_j} \left(\xi_{iq}^I \xi_{jk}^I \xi_k + \xi_{iq}^I \xi_{jl}^I \xi_l \right)$$

$$\frac{\partial v_p}{\partial x_j} = 0$$

$$\frac{\partial v_q}{\partial x_j} = 0$$

for $j = 1,2,3$. The nonzero expression above amounts to

$$\frac{\partial v_i}{\partial x_i} = \frac{2}{l_i} \xi_q$$

$$\frac{\partial v_i}{\partial x_p} = 0$$

$$\frac{\partial v_i}{\partial x_q} = \frac{2}{l_q} \xi_i .$$

Notable here is that a pure bending mode gives arise to a (spurious) transverse shear strain represented by the last expression in the above. Assuming that l_q is small compared to l_i it goes without saying that this term may dominate the internal energy and this is the source to what can be denoted *transverse shear locking*.

4 Solid element type -2

Given this insight the modifications in the expression of the jacobian matrix are as follows. Let

$$\kappa_{mn} = \min(1, \frac{\sqrt{J_{1m}^0 J_{1m}^0 + J_{2m}^0 J_{2m}^0 + J_{3m}^0 J_{3m}^0}}{\sqrt{J_{1n}^0 J_{1n}^0 + J_{2n}^0 J_{2n}^0 + J_{3n}^0 J_{3n}^0}})$$

be the aspect ratio between dimensions m and n at time zero. The modified jacobian is written

$$\tilde{J}_{ij} = x_{Ii} \frac{1}{8} \left(\xi_j^I + \xi_{jk}^I \xi_{ki} + \xi_{jl}^I \xi_{li} + \xi_{123}^I \xi_{ki} \xi_{li} \right)$$

where

$$\xi_{ki} = \begin{cases} \xi_k \kappa_{jk} & i \neq j \\ \xi_k & \text{otherwise} \end{cases}$$

and

$$\xi_{li} = \begin{cases} \xi_l \kappa_{jl} & i \neq j \\ \xi_l & \text{otherwise} \end{cases}.$$

The velocity gradient is now given as

$$L_{ij} = \dot{\tilde{J}}_{ik} \tilde{J}_{kj}^{-1} = \tilde{B}_{ijIk} v_{Ik}$$

where $\tilde{B}_{ijIk}$ is the gradient-displacement matrix for solid element type -2 in LS-DYNA. The same procedure described in Section 2 is used to prevent volumetric locking.

5   Transverse shear locking example revisited

Once again let's look at the parallelepiped of dimensions $l_1 \times l_2 \times l_3$. The jacobian matrix is still diagonal and the velocity gradient is with the new element formulation expressed as

$$L_{ij} = \frac{2}{l_j} \dot{\tilde{J}}_{ij} = \frac{1}{4l_j} v_{Ii} \left(\xi_j^I + \xi_{jk}^I \xi_{ki} + \xi_{jl}^I \xi_{li} + \xi_{123}^I \xi_{ki} \xi_{li} \right)$$

where, again, $k = 1 + \mathrm{mod}(j,3)$ and $l = 1 + \mathrm{mod}(j+1,3)$. The velocity gradient for a pure bending mode is now given as

$$L_{ij} = \frac{1}{4l_j} \left(\xi_{iq}^I \xi_{jk}^I \xi_{ki} + \xi_{iq}^I \xi_{jl}^I \xi_{li} \right)$$

which amounts to (for the potential nonzero elements)

$$L_{ii} = \frac{2}{l_i} \xi_q$$

$$L_{ip} = 0$$

$$L_{iq} = \frac{2}{l_q} \xi_i \kappa_{qi}.$$

If we assume that this is the geometry in the beginning of the simulation and that l_q is smaller than l_i the transverse shear strain can be expressed as

$$L_{iq} = \frac{2}{l_i} \xi_i$$

meaning that the transverse shear energy is not affected by poor aspect ratios, i.e., the transverse shear strain does not grow with decreasing l_q.

6   Solid element type -1

Working out the details in the expression of the gradient-displacement matrix for solid element type -2 reveals that this matrix is dense, i.e., there are 216 nonzero elements in this matrix that needs to be processed compared to 72 for the standard solid element type 2. A slight modification of the jacobian matrix will substantially reduce the computational expense for this element. Simply substitute the expressions for ξ_{ki} and ξ_{li} in Section 4 by

$$\xi_{ki} = \xi_k \kappa_{jk}$$

and

$$\xi_{li} = \xi_l \kappa_{jl}.$$

This will lead to a stiffness reduction for certain modes, in particular the out-of-plane hourglass mode as can be seen by once again looking at the transverse shear locking example. The velocity gradient for pure bending is now

$$L_{ii} = \frac{1}{4l_i} \xi_q \kappa_{iq}$$

$$L_{ip} = 0$$

$$L_{iq} = \frac{1}{4l_q} \xi_i \kappa_{qi}$$

and if it turns out that l_i is smaller than l_q, then this results in

$$L_{ii} = \frac{1}{4l_q} \xi_q .$$

That is, if i represents the direction of the thinnest dimension, its corresponding bending strain is inadequately reduced.
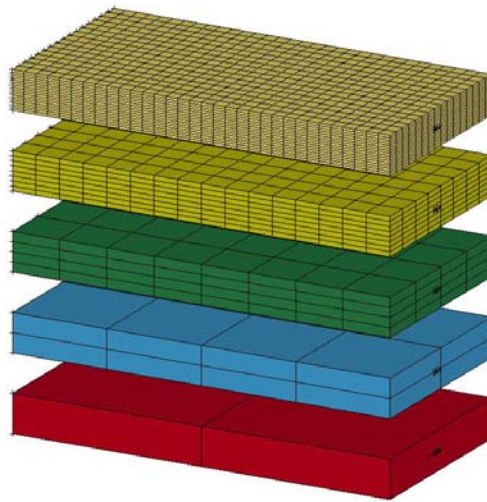

Figure 2 Implicit elastic bending of plate with poor element aspect ratio, different mesh discretizations

7   Examples

7.1   Implicit elastic bending

A plate of dimensions $10x5x1\,mm^3$ is clamped at one end and subjected to a $1\,Nm$ torque at the other end, see Figure 2. The Young's modulus is $210\,GPa$ and the analytical solution for the end tip deflection is $0.57143\,mm$. In order to study the mesh convergence for the three fully integrated bricks the plate is discretized into $2x1x1$, $4x2x2$, $8x4x4$, $16x8x8$ and finally $32x16x16$ elements, all elements having the same aspect ratio of $5:1$.

Table 1 End tip deflection for different mesh discretizations and element types, error in parenthesis.

Discretization	Solid element type 2	Solid element type -2	Solid element type -1
2x1x1	0.0564 (90.1%)	0.6711 (17.4%)	0.6751 (18.1%)
4x2x2	0.1699 (70.3%)	0.5466 (4.3%)	0.5522 (3.4%)
8x4x4	0.3469 (39.3%)	0.5472 (4.2%)	0.5500 (3.8%)
16x8x8	0.4820 (15.7%)	0.5516 (3.5%)	0.5527 (3.3%)
32x16x16	0.5340 (6.6%)	0.5535 (3.1%)	0.5540 (3.1%)

In Table 1 the results for the different mesh discretizations as well as element types are given, and it can be concluded that the new elements are substantially less stiff than the type 2 element and also quite accurate for that matter.
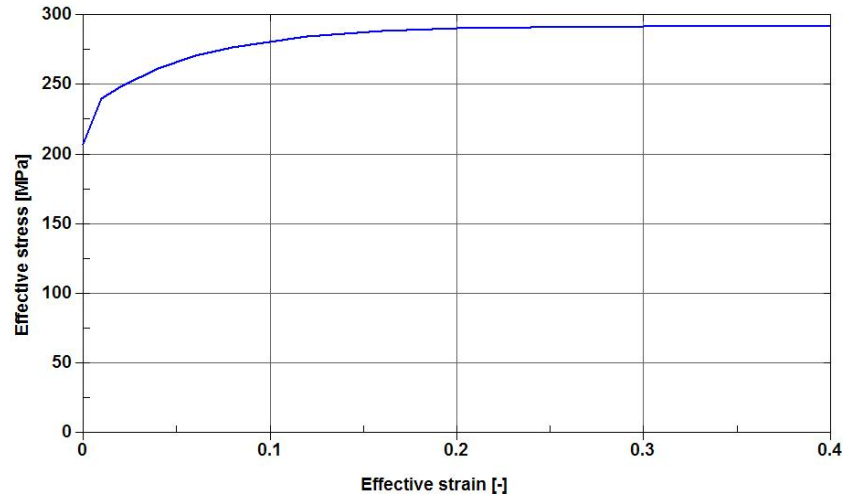
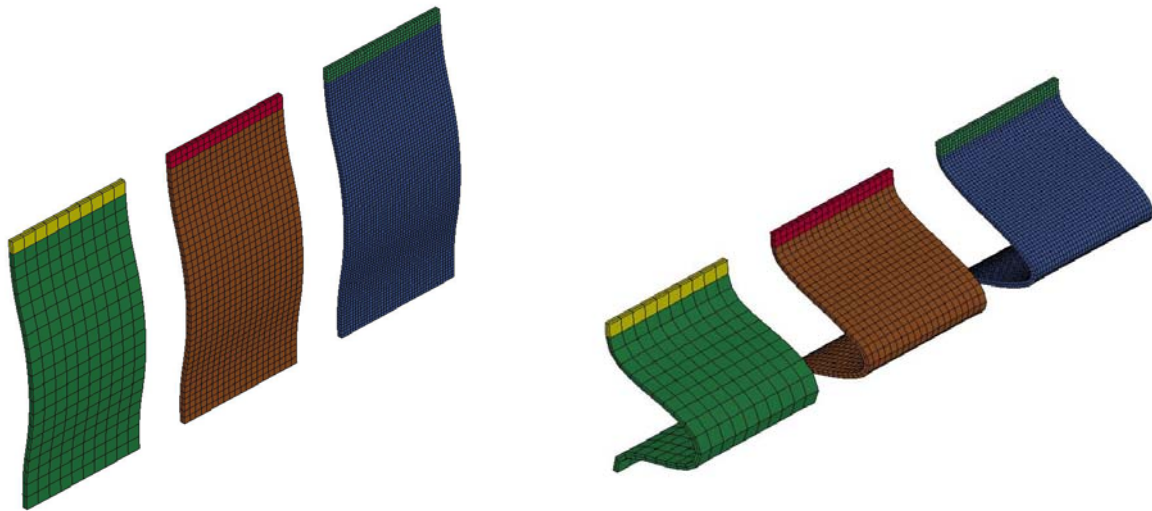*Figure 3 Hardening curve for material used in the strip and tube example.*

Figure 4 Initial and final configuration of strip, different mesh discretizations

7.2   Plastic buckling of strip

An initially imperfected plate strip of dimensions $100x50x2\,mm^3$ is fixed at one end and at the other subjected to a prescribed motion of $1\,m/s$ for the duration of $0.05\,s$ so that it deforms according to Figure 4. The material used is AA 6063 T6 from [2] for which the density is $3000\,kg/m^3$, Young's modulus is $68.3\,GPa$, Poisson's ratio is 0.3 and the hardening curve is shown in Figure 3. Three different mesh discretizations are used, all having two elements through the thickness and thus the aspect ratio varies between $5:1$, $5:2$ and $5:4$. For this problem we measure the internal+hourglass energy and use the result from solid element type 1 as a reference to compare with. In Figure 5 the mesh convergence is shown for the different element types. While element type 2 converges rather slow with mesh refinement, the new element types seem to be more or less insensitive to mesh size and compare well with element type 1.
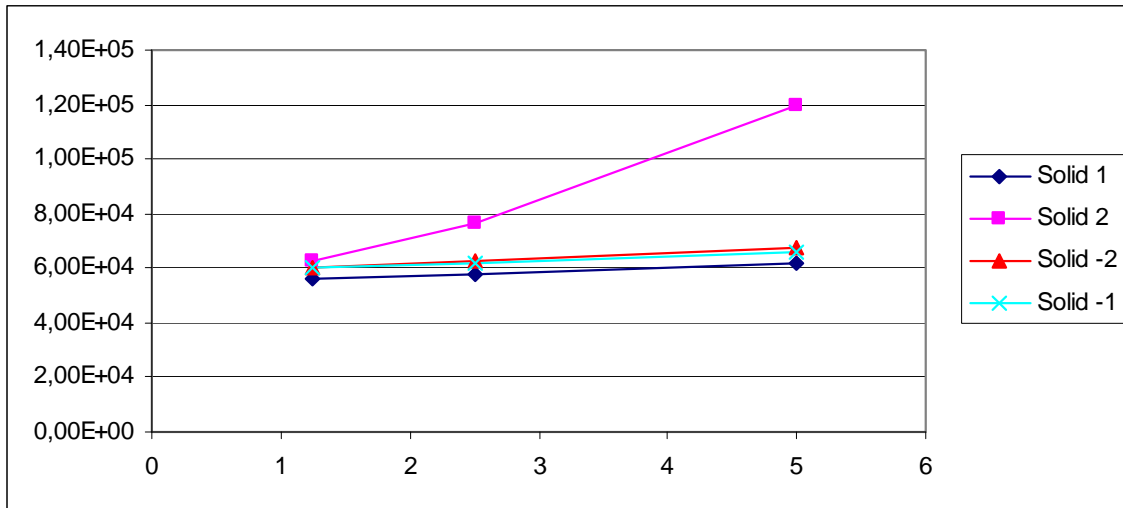
Figure 5 Graphs showing internal energy (y-axis) for strip with different element aspect ratio (x-axis) and element types (legend).

7.3   Plastic buckling of rectangular tube

In order to check the accuracy for more general deformation modes a tube of height $70\,mm$, rectangular cross section of $80x80\,mm^2$ and wall thickness of $2\,mm$ is fixed at one end and at the other subjected to a prescribed motion of $5\,m/s$ for the duration of $0.01\,s$ so that it deforms according to Figure 6. Symmetry conditions are used to model only one quarter of the tube and initiators are used to trigger the deformation. The same material as in the previous example is used, and this time we use one coarse and one fine discretization. The coarse discretization is with 2 elements through the wall thickness and the fine is with 4 elements through the wall thickness. The aspect ratio varies between $5:1$, $3:1$, $2:1$ and $1:1$ for both set of mesh discretizations, only the coarse discretization is illustrated in Figure 6. In Figure 7 the results in terms of final internal+hourglass energy are shown for the different element types and aspect ratio, and again it appears that solid element types -1 and -2 converge faster than element type 2. Notable is that element type 1 gives a stiffer response for this problem. We believe this is due to the use of an elastic hourglass formulation and that there is a substantial amount of hourglass deformation in the corners of the tube.

8   Conclusions

In LS-DYNA, two new selective reduced integrated hexahedral elements are available that should be seen as alternatives to solid element type 2 for problems with poor element aspect ratio. The typical situation when the latter arises is when thin walled structures require solid element modelling and the mesh density must be kept at a minimum for efficiency reasons. The new elements are termed solid element type -1 and type -2, and they are derived from solid element type 2 by modifying its jacobian matrix in a heuristic manner to reduce the transverse shear stiffness for pure bending modes. The modification can be partially justified from a theoretical viewpoint but results show that they also work well in practice. The expense for using the new elements is a reduction in computational efficiency, and experiments indicate that solid element type -2 has a cost of about 3.5 times solid element 2 whereas for solid element type -1 this number is as low as 1.2. Even though element type -2 is the theoretically more sound element, the numerical examples have shown no signs of solid element type -1 giving worse results. One should be aware however that there is a stiffness reduction in the out-of-plane hourglass mode that could result in slightly more hourglassing which is illustrated in Figure 8 for the rectangular tube example. Nevertheless, given its proved accuracy and computational efficiency we find it reasonable to recommend using solid element type -1 in favour of solid element type -2 for explicit analyses. For large scale implicit analyses the influence of element processing should be small enough when compared to the expense of solving the linear system of equations that either one of the two elements could be used.
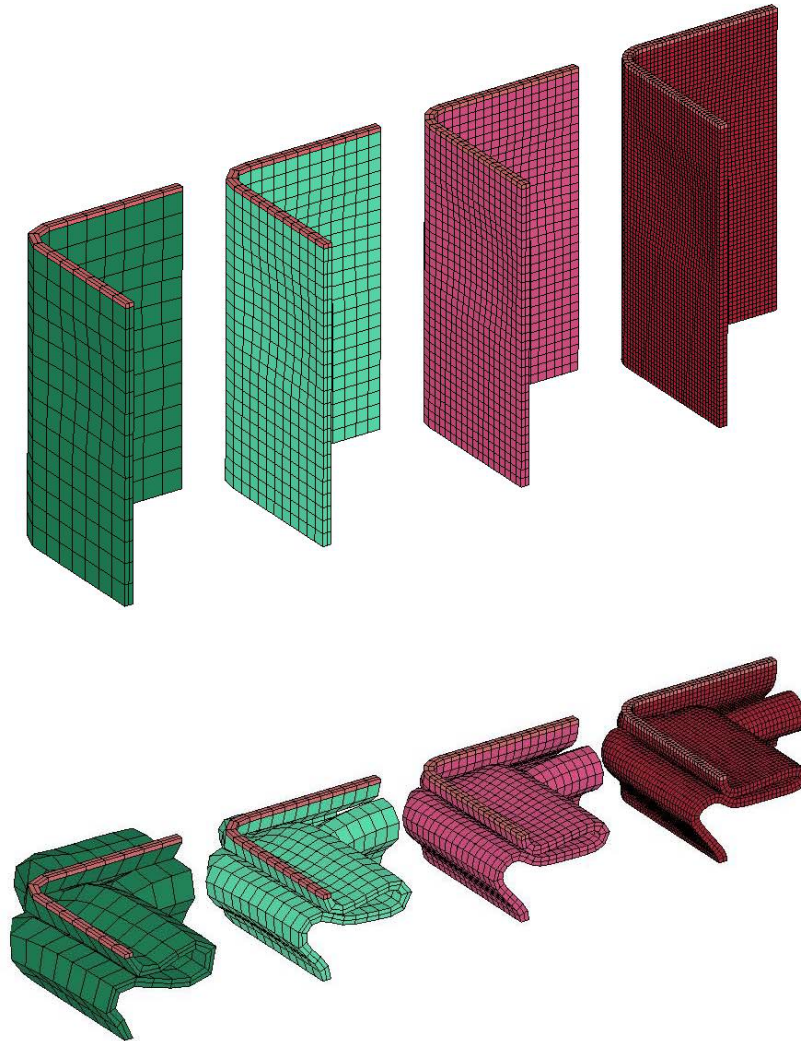
Figure 6 Initial and final configuration of rectangular tube with symmetry conditions, different mesh discretizations

9   Acknowledgments

The author would like to thank Anders Jernberg and Mikael Jansson of Engineering Research Nordic AB for helping out with the numerical examples.

10   Literature

[1] LS-DYNA Keyword User's Manual Version 971, Volume I-II, Livermore Software Technology Corporation (LSTC), Livermore CA, 2007.

[2] Achani, D: "Constitutive models of elastoplasticity and fracture for aluminium alloys under strain path change", Doctoral Thesis, 2006-76, NTNU Trondheim, Norway.
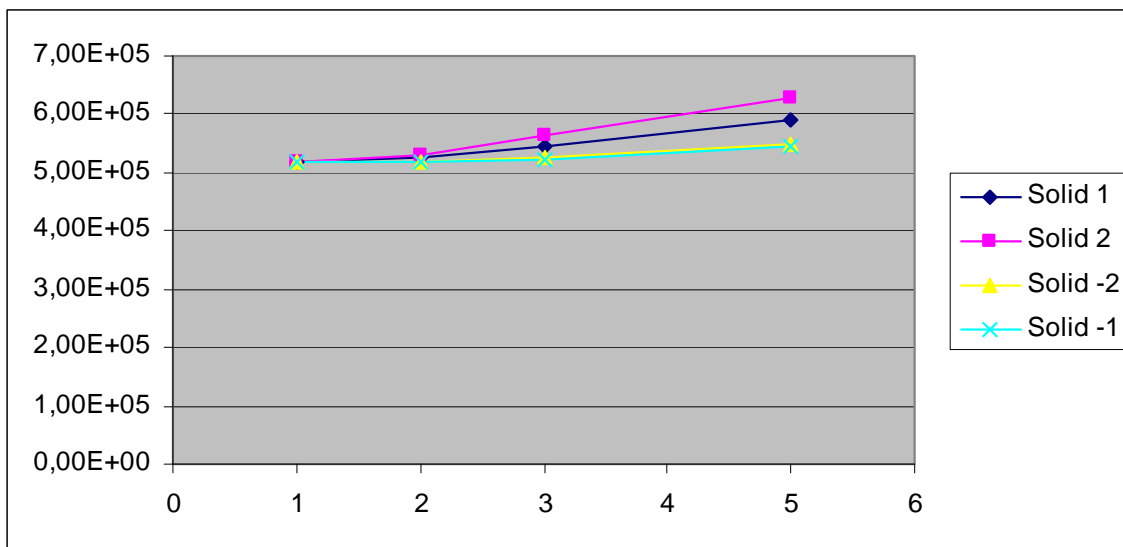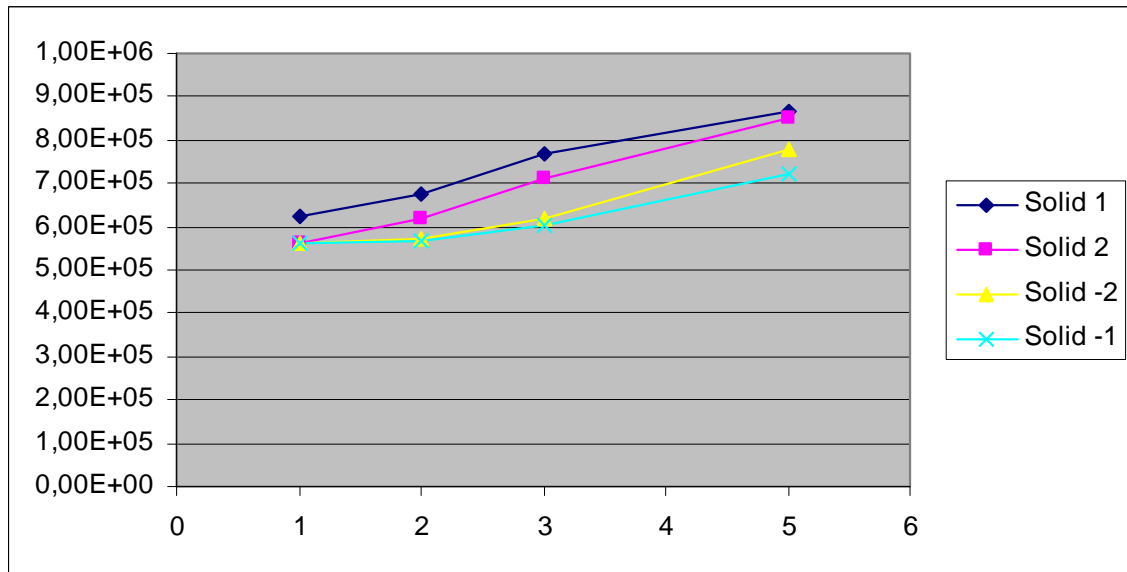
Figure 7 Graphs showing internal energy (y-axis) for tube with different element aspect ratio (x-axis), mesh discretizations (coarse above and fine below) and element types (legend).
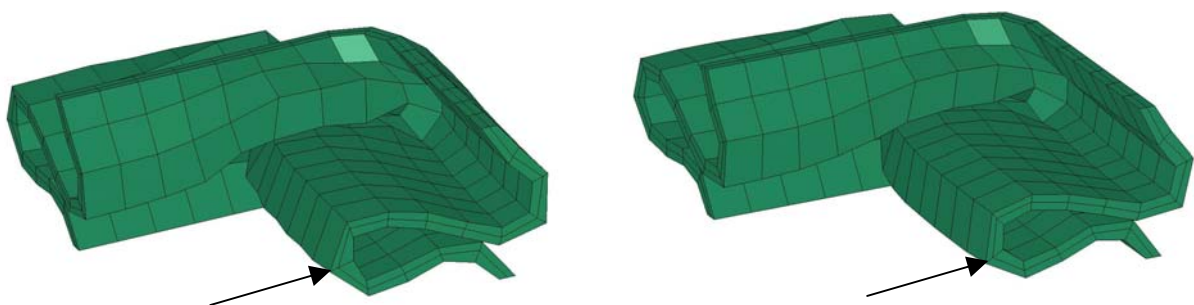

Figure 8 Illustration of the stiffness reduction in out-of-plane hourglass modes for solid element type -1 (left) when compared to solid element type -2 (right).